Title

Protein arginine methyltransferase 3 fine-tunes the assembly/disassembly of pre-ribosomes to repress nucleolar stress by interacting with RPS2B in arabidopsis

Journal

Molecular Plant, 14(2)

ISSN

1674-2052

Authors

Hang, Runlai
Wang, Zhen
Yang, Chao
et al.

Publication Date

2021-02-01

DOI

10.1016/j.molp.2020.10.006

Peer reviewed

Molecular Plant
Research Article

CellPress
Partner Journal

Protein arginine methyltransferase 3 fine-tunes the assembly/disassembly of pre-ribosomes to repress nucleolar stress by interacting with RPS2B in *arabidopsis*

Runlai Hang[1,3,4,6], Zhen Wang[1,2,6], Chao Yang[1,2], Lilan Luo[1], Beixin Mo[3], Xuemei Chen[4], Jing Sun[1,*], Chunyan Liu[1,*] and Xiaofeng Cao[1,2,5,*]

[1]State Key Laboratory of Plant Genomics and National Center for Plant Gene Research, Institute of Genetics and Developmental Biology, Chinese Academy of Sciences, Beijing 100101, China

[2]College of Life Sciences, University of Chinese Academy of Sciences, Beijing 100039, China

[3]Guangdong Provincial Key Laboratory for Plant Epigenetics, College of Life Sciences and Oceanography, Shenzhen University, Shenzhen 518060, China

[4]Department of Botany and Plant Sciences, Institute of Integrative Genome Biology, University of California, Riverside, Riverside, CA 92521, USA

[5]CAS Center for Excellence in Molecular Plant Sciences, Chinese Academy of Sciences, Beijing 100101, China

[6]These authors contributed equally to this article.

***Correspondence: Jing Sun (jsun@genetics.ac.cn), Chunyan Liu (cyliu@genetics.ac.cn), Xiaofeng Cao (xfcao@genetics.ac.cn)**

https://doi.org/10.1016/j.molp.2020.10.006

ABSTRACT

Ribosome biogenesis, which takes place mainly in the nucleolus, involves coordinated expression of pre-ribosomal RNAs (pre-rRNAs) and ribosomal proteins, pre-rRNA processing, and subunit assembly with the aid of numerous assembly factors. Our previous study showed that the *Arabidopsis thaliana* protein arginine methyltransferase AtPRMT3 regulates pre-rRNA processing; however, the underlying molecular mechanism remains unknown. Here, we report that AtPRMT3 interacts with Ribosomal Protein S2 (RPS2), facilitating processing of the 90S/Small Subunit (SSU) processome and repressing nucleolar stress. We isolated an intragenic suppressor of *atprmt3-2*, which rescues the developmental defects of *atprmt3-2* while produces a putative truncated AtPRMT3 protein bearing the entire N-terminus but lacking an intact enzymatic activity domain We further identified RPS2 as an interacting partner of AtPRMT3, and found that loss-of-function *rps2a2b* mutants were phenotypically reminiscent of *atprmt3*, showing pleiotropic developmental defects and aberrant pre-rRNA processing. RPS2B binds directly to pre-rRNAs in the nucleus, and such binding is enhanced in *atprmt3-2*. Consistently, multiple components of the 90S/SSU processome were more enriched by RPS2B in *atprmt3-2*, which accounts for early pre-rRNA processing defects and results in nucleolar stress. Collectively, our study uncovered a novel mechanism by which AtPRMT3 cooperates with RPS2B to facilitate the dynamic assembly/disassembly of the 90S/SSU processome during ribosome biogenesis and repress nucleolar stress.

Key words: AtPRMT3, RPS2, ribosome assembly, pre-rRNA processing, 90S/SSU processome, nucleolar stress

Hang R., Wang Z., Yang C., Luo L., Mo B., Chen X., Sun J., Liu C., and Cao X. (2021). Protein arginine methyltransferase 3 fine-tunes the assembly/disassembly of pre-ribosomes to repress nucleolar stress by interacting with RPS2B in *arabidopsis*. Mol. Plant. **13**, 223–236.

INTRODUCTION

Protein arginine methyltransferase 3 (PRMT3) is a conserved type I protein arginine methyltransferase catalyzing the formation of asymmetric dimethylarginine (Tang et al., 1998; Bedford and Clarke, 2009; Liu et al., 2010; Ahmad and Cao, 2012). Deletion of the PRMT3 homolog in fission yeast affects the ratio of 40S to 60S free ribosomal subunits without disturbing precursor ribosomal RNA (pre-rRNA) processing (Bachand and Silver, 2004). In mice, PRMT3-deficient embryos are small in size, but the levels of 40S, 60S, and 80S monosome and polyribosomes are unaffected (Swiercz et al., 2007). In yeast and mammals, PRMT3 methylates

Published by the Molecular Plant Shanghai Editorial Office in association with Cell Press, an imprint of Elsevier Inc., on behalf of CSPB and CEMPS, CAS.

Ribosomal Protein S2 (RPS2) (Bachand and Silver, 2004; Swiercz et al., 2005, 2007); however, the RMT3–RPS2 interaction, rather than the methyltransferase activity of RMT3, is essential for ribosomal small subunit maturation (Perreault et al., 2009). AtPRMT3 is required for ribosome biogenesis at the level of pre-rRNA processing, where it balances the two alternative pre-rRNA processing pathways (Hang et al., 2014), which differ in the order of 5′ external transcribed spacer (ETS) removal and internal transcribed spacer (ITS1) cleavage (Hang et al., 2014; Weis et al., 2015a; Saez-Vásquez and Delseny, 2019).

The membrane-less nucleolus, where rDNA transcription, rRNA processing, and ribosome assembly occur, is the primary location for ribosome biogenesis (Woolford and Baserga, 2013). Ribosome assembly is a fundamental and highly sophisticated process involving not only rRNAs and ribosomal proteins but also many assembly factors and small nucleolar RNAs (snoRNAs) (Henras et al., 2008; Woolford and Baserga, 2013; Lafontaine, 2015). In the early stage of pre-rRNA processing, the primary rRNA transcripts are assembled co-transcriptionally with ribosomal proteins and assembly factors to form the 90S/SSU processome (Dragon et al., 2002; Grandi et al., 2002; Osheim et al., 2004). The U3 small nucleolar ribonucleoprotein (snoRNP) complex is an essential component of the 90S/SSU processome, which is required for nucleolar processing of 18S rRNA precursors (pre-18S rRNA) (Dragon et al., 2002; Watkins and Bohnsack, 2012). Base pairing of the U3 snoRNA with the 5′ ETS and pre-18S rRNA helps the 90S/SSU processome mediate early pre-rRNA folding and cleavage within the 5′ ETS and ITS1 (Sharma and Tollervey, 1999; Dutca et al., 2011; Marmier-Gourrier et al., 2011). Cleavage of 35S rRNA transcripts at site A2 in yeast splits the 90S/SSU processome into pre-40S and pre-60S particles (Thomson et al., 2013). In higher plants, the U3 snoRNP was first characterized as the Nuclear Factor D (NF-D) complex in cauliflower inflorescences (Sáez-Vásquez et al., 2004a, 2004b) and later as the BoU3 (*B. oleracea* U3) complex from *Brassica oleracea* (Samaha et al., 2010). The NF-D/BoU3 complex recruited by A123B (A(1), A(2), A(3), and B motifs) contributes to P-site cleavage in the 5′ ETS region (Caparros-Ruiz et al., 1997; Sáez-Vásquez et al., 2004a, 2004b; Samaha et al., 2010). Ribosomal proteins are indispensable for ribosome biogenesis, shuttling into the nucleus where they incorporate into pre-ribosomes coordinately and sequentially (de la Cruz et al., 2015). For example, RPS2 in fission yeast participates in pre-rRNA processing and nuclear export of pre-40S subunits (Perreault et al., 2008). Defects in any of the components involved in ribosome biogenesis usually result in a disordered nucleolus structure, which can induce nucleolar stress at the cellular level (Zhang and Lu, 2009; Boulon et al., 2010; Ohbayashi and Sugiyama, 2017).

Ribosome biogenesis is seamlessly orchestrated to ensure normal growth and development. Defects in ribosome biogenesis lead to severe biological consequences, such as ribosomopathies in humans (Narla and Ebert, 2010). In *Arabidopsis*, some null mutants of ribosome-related genes are embryo lethal or show pleiotropic developmental defects (Byrne, 2009; Horiguchi et al., 2011; Weis et al., 2015a). For example, factors involved in SSU maturation such as SLOW WALKER 1 (SWA1, a homolog of yeast UTP15) (Shi et al., 2005), PERIODIC TRYPTOPHAN PROTEIN 2 (PWP2) (Missbach et al., 2013), and YAO (a homolog of yeast Ribosomal RNA Processing protein 9, RRP9) (Li et al., 2010) are essential for gametophyte development in *Arabidopsis*. Plant ribosome biogenesis is affected by different kinds of factors, such as RRP7 (Micol-Ponce et al., 2018), NUCLEOLIN (Kojima, et al., 2007; Pontvianne et al., 2007), histone deacetylases HD2B and HD2C (Chen et al., 2018, 2020), the snoRNA *HIDDEN TREASURE 2* (*HID2*) (Zhu et al., 2016), ribosomal protein RPL4A (Rosado et al., 2010), and the putative methyltransferase ROOT INITIATION DEFECTIVE 2 (RID2) (Ohbayashi et al., 2011). Mutants of these factors produce phenotypes common to mutants of ribosomal proteins and related factors, including retarded growth and narrow, pointed leaves.

In this study, we reported the isolation of an intragenic suppressor of *atprmt3-2*, which produces a truncated AtPRMT3 protein lacking an intact enzymatic domain at the C terminus, and showed that the N terminus of AtPRMT3 is required for its biological functions. We then identified the *Arabidopsis* RPS2 family members as interaction partners of AtPRMT3. The *rps2a2b* mutants displayed developmental defects similar to those of *atprmt3-2* mutants. RNA immunoprecipitation (RIP) assays showed that AtPRMT3 affected the association of RPS2B with pre-rRNAs in the nucleus. Dysfunction of AtPRMT3 resulted in enhanced association between RPS2B and the 90S/SSU processome and nucleolar stress as evidenced by enlarged nucleoli in *atprmt3-2* mutants.

RESULTS

The Enzymatic Domain of AtPRMT3 Is Dispensable for Its Biological Function

AtPRMT3 is required for proper pre-rRNA processing, but the underlying molecular mechanism remains elusive (Hang et al., 2014). To address this question, we performed a genetic screen for suppressors of the *atprmt3-2* mutant, which is a null mutant with a T-DNA insertion in the fifth intron (Hang et al., 2014). Seeds of *atprmt3-2* were mutagenized with ethylmethanesulfonate (EMS), and four dominant suppressors rescuing the pleiotropic phenotypes of *atprmt3-2*, namely *m15*, *m21*, *m206*, and *b3*, were isolated (Supplemental Figure 1A). By performing whole-genome resequencing, we found that *m15*, *m21*, and *m206* exhibited the same intragenic G-to-A nucleotide mutation upstream of the T-DNA insertion site of *atprmt3-2*; this mutation converts tryptophan-366 into a stop codon (W366*) and is referred to as *atprmt3-R1* hereafter (Figure 1A and Supplemental Figure 1B). Furthermore, by performing Sanger sequencing we identified a new intragenic C-to-T mutation converting glutamine-353 into a stop codon (Q353*) in *b3*, which is referred to as *atprmt3-R2* hereafter (Figure 1A). RT–PCR indicated that the *AtPRMT3* transcript upstream of the T-DNA insertion site, rather than the full-length transcript, was present in *atprmt3-2 atprmt3-R1, atprmt3-2 atprmt3-R2*, and *atprmt3-2* (Supplemental Figure 1C). Interestingly, immunoblotting with anti-AtPRMT3 suggested that the truncated N-terminal part of AtPRMT3 was successfully translated in these two dominant suppressor lines, *atprmt3-2 atprmt3-R1* and *atprmt3-2 atprmt3-R2* (Figure 1B).

The intragenic mutation (W366*) in *atprmt3-R1* is located in the Double E domain, which is essential for PRMT enzymatic activity, and is conserved in different species (Supplemental Figure 1D). In

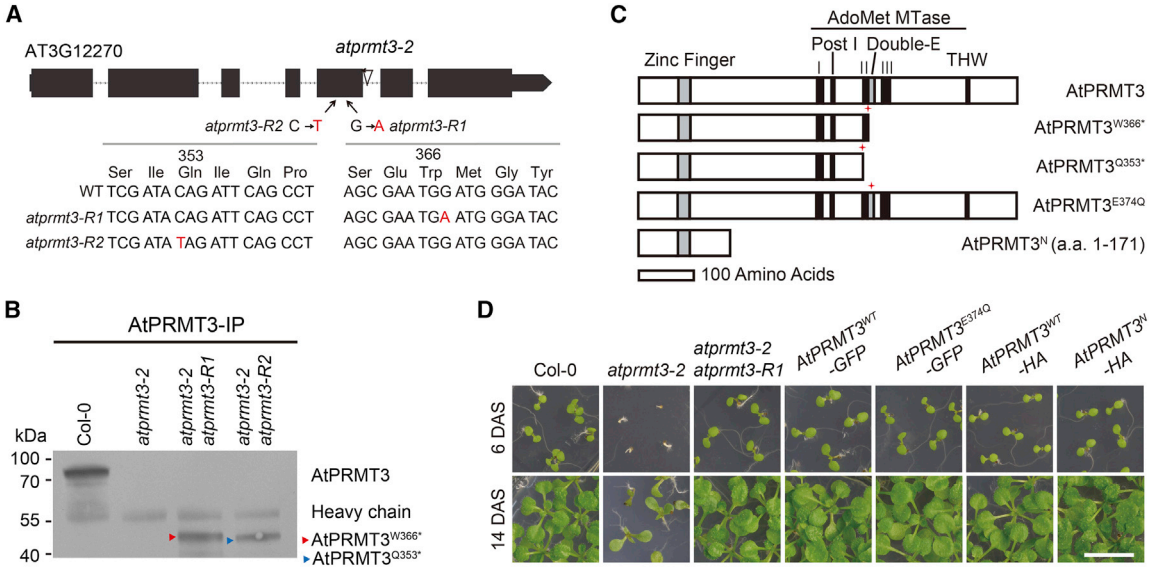

Figure 1. The N Terminus of AtPRMT3 Rather Than Its Enzymatic Domain Can Rescue the Developmental Defects of *atprmt3-2*.

(A) Overview of *atprmt3-R1* and *atprmt3-R2* mutations in a schematic diagram of the *AtPRMT3* gene. In *atprmt3-R1*, a G-to-A mutation in the fifth exon changes a Trp (W) to a stop codon (*) at amino acid position 366. In *atprmt3-R2*, a C-to-T mutation in the fifth exon changes a Gln (Q) to a stop codon (*) at amino acid position 353.

(B) *atprmt3-2 atprmt3-R1* and *atprmt3-2 atprmt3-R2* express truncated proteins. Immunoprecipitation (IP) with anti-AtPRMT3 antibodies was performed using total protein lysates from Col-0, *atprmt3-2*, *atprmt3-2 atprmt3-R1*, and *atprmt3-2 atprmt3-R2*. Immunoblotting was then performed with anti-AtPRMT3. Red triangle indicates AtPRMT3^{W366*} and blue triangle indicates AtPRMT3^{Q353*}.

(C) Schematic structures of wild type and mutant AtPRMT3 proteins.

(D) Rescue of retarded growth and pointed first true leaf phenotypes of *atprmt3-2*. *AtPRMT3^{WT}-GFP*, *AtPRMT3^{E374Q}-GFP*, *AtPRMT3^{WT}-HA*, and *AtPRMT3^{N}-HA* indicate complementation lines in the *atprmt3-2* mutant background. DAS, days after stratification. Scale bar, 10 mm.

atprmt3-R1 and *atprmt3-R2*, the enzymatic domain of AtPRMT3 is disrupted. To further verify that the enzymatic activity is dispensable for the biological function of AtPRMT3, we introduced the E374Q point mutation into the Double E domain (Figure 1C); this mutation completely abolished the *in vitro* enzymatic activity of AtPRMT3 against calf thymus core histones (Supplemental Figure 2A) and myelin basic protein (Supplemental Figure 2B). Consistent with the hypothesis that the enzymatic domain in the C terminus is not essential for the biological function of AtPRMT3, AtPRMT3^{E374Q} rescued the developmental defects (Figure 1D; Supplemental Figure 2C and 2D) and aberrant pre-rRNA processing of *atprmt3-2* (Supplemental Figure 3C). Furthermore, we found that a shorter N-terminal region of AtPRMT3 (amino acids 1–171) containing the C2H2 zinc finger (AtPRMT3^{N}) (Figure 1C), is sufficient to rescue the abnormal developmental phenotypes (Figure 1D; Supplemental Figure 2C and 2D) and pre-rRNA processing defects of *atprmt3-2* (Supplemental Figure 3C). These data show that the N-terminal region of AtPRMT3 containing the C2H2 zinc finger, rather than enzymatic activity, is sufficient for its biological functions; this region might function by mediating protein interactions.

AtPRMT3 Physically Interacts with RPS2 Family Proteins

To identify physically interacting partners of AtPRMT3 *in vivo*, we characterized proteins co-immunoprecipitating with AtPRMT3 by liquid chromatography coupled with tandem mass spectrometry (LC–MS/MS) (Supplemental Figure 4A). The RPS2 (uS5) protein family members (Ban et al., 2014) were immunoprecipitated by AtPRMT3 (Figure 2A and Supplemental Table 1). As structural components of the cytoplasmic 80S ribosome, RPS2 proteins are conserved in eukaryotes (Supplemental Figure 5). The *Arabidopsis RPS2* family comprises six genes: *RPS2A* (AT1G58380), three tandem *RPS2B* genes (AT1G58684, AT1G58983, and AT1G59359, which are adjacent to *RPS2A*), *RPS2C* (AT2G41840), and *RPS2D* (AT3G57490) (Supplemental Figure 6A). These genes produce the RPS2A/B/C/D proteins, respectively. These four RPS2 proteins share the same domain structures with an N-terminal arginine/glycine-rich (RGG/RG) motif and a C-terminal Ribosomal_S5 domain (Supplemental Figure 6B). Moreover, their amino acid sequences are highly conserved: RPS2B, RPS2C, and RPS2D share 99%, 92%, and 95% identity with RPS2A, respectively (Supplemental Figure 6C).

The physical associations between AtPRMT3 and each RPS2 protein were further validated by *in vitro* pull-down (Figure 2B) and *in vivo* co-immunoprecipitation (coIP) assays (Figure 2C and Supplemental Figure 4B). Moreover, AtPRMT3^{N} was sufficient for protein interactions with RPS2 both *in vitro* (Supplemental Figure 4C) and *in vivo* (Figure 2D). When the nuclei were treated with harsher lysis conditions (stronger sonication and higher concentration of detergent) to release more proteins, we found that in addition to the cytoplasm, the major site of AtPRMT3 localization, AtPRMT3 also localized in the nucleus (Supplemental Figure 4D). AtPRMT3 and RPS2 interaction can occur in both the cytoplasm and nucleus (Supplemental Figure 4E), which was consistent with the

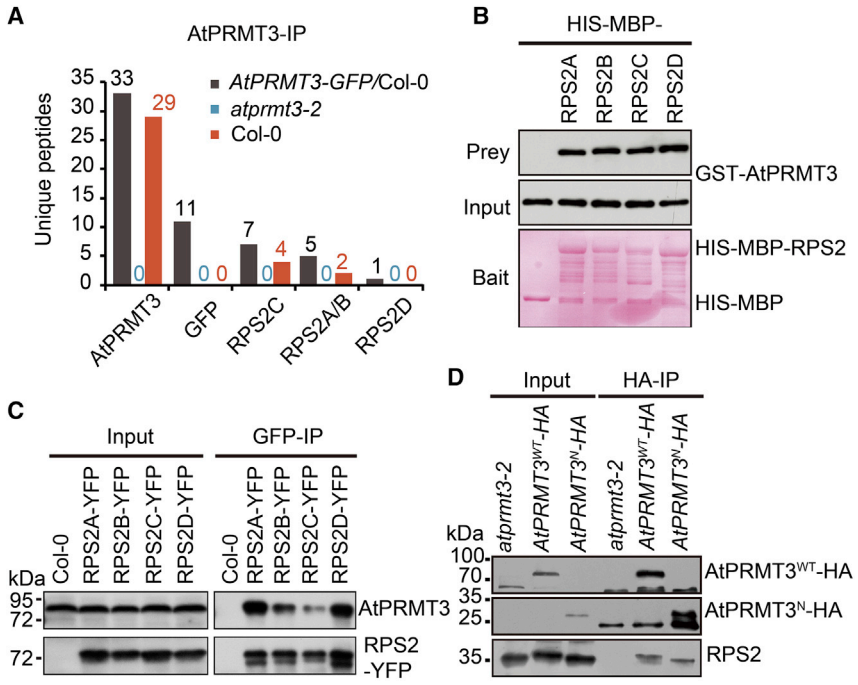

Figure 2. AtPRMT3 Physically Interacts with RPS2 Family Proteins.

(A) RPS2 family proteins co-immunoprecipitated with AtPRMT3. The counts of unique peptides enriched by IP with anti-AtPRMT3 from protein lysates of *AtPRMT3-GFP*/Col-0 (black), *atprmt3-2* (blue), and Col-0 (red) seedlings are shown in the histogram.

(B and C) The interaction of AtPRMT3 and RPS2 family proteins was detected by pull-down assay *in vitro* **(B)** and coIP assay *in vivo* **(C)**. Purified HIS-MBP and HIS-MBP-RPS2A/B/C/D proteins were immobilized on Ni-charged HIS beads as bait, shown by Ponceau S staining. GST-AtPRMT3 was the prey and was detected by anti-GST. Equivalent amounts of input GST-AtPRMT3 were loaded for each pull-down assay **(B)**. Total protein lysates from seedlings of *RPS2A/B/C/D-YFP* in the Col-0 background were subjected to IP using anti-GFP. RPS2-YFP and endogenous AtPRMT3 were detected using antibodies against GFP and AtPRMT3, respectively **(C)**.

(D) AtPRMT3^{N} interaction with RPS2 *in vivo* validated by coIP assay. Total protein lysates from seedlings of *atprmt3-2* and *atprmt3-2* complementation lines *AtPRMT3^{WT}-HA* and *AtPRMT3^{N}-HA* were subjected to IP using anti-HA. RPS2 and AtPRMT3 were detected with anti-RPS2B-N and anti-HA antibodies, respectively.

results of a bimolecular fluorescence complementation assay (Supplemental Figure 4F).

Disruption of *RPS2A2B* Produced Developmental and Pre-rRNA Processing Defects as Observed in *atprmt3* Mutants

To check whether RPS2 family members play important roles in plant growth and development, we obtained T-DNA insertion mutants or created genetic mutants via the CRISPR/Cas9 approach. It was obvious that neither the T-DNA insertion allele *rps2c-1* for *RPS2C* (Supplemental Figure 7E and 7F) nor gene-editing alleles *rps2d-1* and *rps2d-2* for *RPS2D* (Supplemental Figure 7G) exhibited pointed first true leaves like *atprmt3-2* (Supplemental Figure 8H). The three identical genes encoding *RPS2B* are physically close to *RPS2A* on chromosome 1 (Supplemental Figure 6A). Besides this, RPS2A and RPS2B show a high degree of sequence identity, differing by only one amino acid (Supplemental Figure 6C). To determine the biological function of *RPS2*, we applied CRISPR/Cas9 technology to knock out *RPS2A* and the three *RPS2B* genes simultaneously, using a common guide RNA (Supplemental Figure 7A). The resulting *rps2a2b-1* mutants were confirmed by DNA sequencing (Supplemental Figure 7B) and immunoblotting (Supplemental Figure 8A).

Intriguingly, the *rps2a2b-1* mutants exhibited pleiotropic developmental defects resembling those of *atprmt3-2*, such as short primary roots (Figure 3A and 3B), pointed first true leaves, disrupted leaf vein patterns (Figure 3C and Supplemental Figure 8B), growth retardation including delayed germination (Supplemental Figure 8C), and delayed cotyledon greening (Supplemental Figure 8D). The developmental defects of *rps2a2b-1* could be rescued by a complementation construct expressing *RPS2B*, but not by one expressing *RPS2A* (Figure 3A–3C and Supplemental Figure 8B–8D). Since RPS2A and RPS2B differ by only one amino acid, we predict that the different abilities of *RPS2A* and *RPS2B* to complement the *rps2a2b-1* mutant may be mainly due to their different expression levels (Supplemental Figure 8A). Consistent with this, the mRNA levels of *RPS2A* were lower than those of *RPS2B* in Columbia-0 (Col-0) (Supplemental Figure 8E). To further validate this hypothesis, we used the promoter of *RPS2B* to drive the expression of *RPS2A* and found that *RPS2B$_{pro}$::RPS2A* could rescue the developmental defects of *rps2a2b-1* (Supplemental Figure 8F and 8G). In addition, the single *rps2a-1* T-DNA insertion mutant did not show any obvious developmental defects (Supplemental Figures 7C, 7D, and 8H). The results suggest that phenotypes of *rps2a2b-1* are mainly caused by the *rps2b* mutations.

To determine the molecular function of RPS2A2B in ribosome biogenesis, we used northern blot assays to evaluate pre-rRNA processing in the *rps2a2b-1* mutants. Steady-state levels of pre-rRNA intermediates were detected by probes as previously described (Hang et al., 2014), and as illustrated in Supplemental Figure 3A and 3B. Compared with wild-type Col-0, the *rps2a2b-1* mutants accumulated more 33S(P′)/32S and 27SA2 (Figure 3D and Supplemental Figure 9A), the markers for "5′ ETS-first" processing. By contrast, levels of P-A3, the marker for "ITS1-first" pre-rRNA processing, were lower in *rps2a2b-1* (Supplemental Figure 9B). This unbalanced pre-rRNA processing pattern in *rps2a2b-1* may result in delayed processing of 18S-A3 in the pre-40S SSU, and 27SA and 27SB in the pre-60S LSU (large subunit) (Figure 3D and Supplemental Figure 9). These pre-rRNA processing defects of *rps2a2b-1* were similar to those of *atprmt3-2* and were also rescued by *RPS2B* but not by *RPS2A* (Figure 3D).

To further decipher the genetic relationship between *AtPRMT3* and *RPS2A2B* in ribosome biogenesis, we carried out genetic

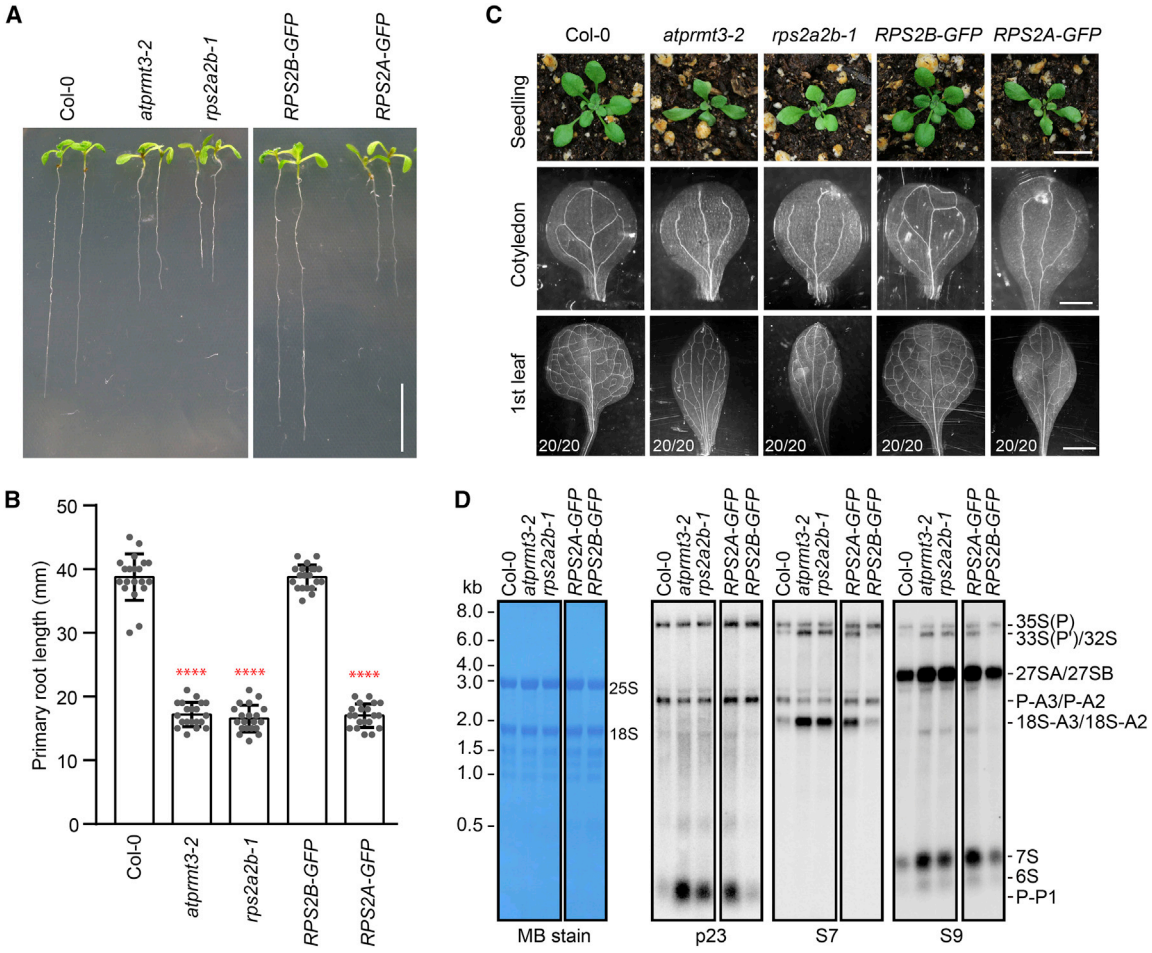

Figure 3. The *rps2a2b* and *atprmt3* Mutants Exhibit Similar Developmental and pre-rRNA Processing Defects.

(A and B) The *rps2a2b-1* mutants exhibited short primary roots resembling those of *atprmt3-2* **(A)**, as supported by statistical data **(B)**. *RPS2A-GFP* and *RPS2B-GFP* indicate complementation lines in the *rps2a2b-1* mutant background. Twenty seedlings were scored for each genetic background. Error bars indicate SD. Student's *t*-test was used to calculate the *P* value. ****$P < 0.0001$. Scale bar, 10 mm.

(C) The *rps2a2b-1* mutants produce pointed first true leaves and aberrant vein patterns in the cotyledons and first true leaves. For each genotype, 20 leaves are recorded and all of them show similar phenotype as indicated in the picture. Scale bar, 10 mm for seedlings (upper), 1 mm for cotyledons (middle), and 2 mm for the first true leaf (lower).

(D) Aberrant pre-rRNA processing in *rps2a2b-1* mutants. Methylene blue staining (MB stain) is shown as a loading control.

crosses between *atprmt3-2* and *rps2a2b-1*. However, we failed to obtain the *atprmt3rps2a2b* triple mutant. Examination of siliques of *atprmt3*(+/−)*rps2a2b*(−/−) plants revealed the presence of aborted ovules (Supplemental Figure 10A). These defective ovules were arrested at the globular embryo stage (Supplemental Figure 10B). The similar developmental and molecular phenotypes of *rps2a2b-1* and *atprmt3-2*, as well as the embryonic lethal phenotypes of *atprmt3 rps2a2b* triple mutants, suggested that RPS2B and AtPRMT3 may function coordinately and redundantly in ribosome biogenesis to promote plant growth and development. Nevertheless, we still cannot exclude the possibility of extra ribosomal activities of RPS2, which will be determined in the future.

Genes Involved in Ribosome Biogenesis Were Overexpressed in *atprmt3* and *rps2a2b* Mutants

To gain further insights into the biological functions of *AtPRMT3* and *RPS2A2B*, we performed transcriptomic analysis of Col-0, *atprmt3-2*, and *rps2a2b-1* by high-throughput sequencing. We obtained 16–20 million clean paired-end reads from each sample, and over 15 million reads from each sample were aligned to the *Arabidopsis* genome (Supplemental Table 3). We identified 2415 upregulated genes and 1329 downregulated genes in *atprmt3-2* compared with Col-0 (Supplemental Figure 11A). Gene Ontology (GO) analysis revealed that the upregulated genes showed significant enrichment in functions related to RNA methylation ($P = 2.11 \times 10^{-31}$), translation ($P = 7.74 \times 10^{-24}$), peptide biosynthetic process ($P = 1.54 \times 10^{-23}$), and ribosome biogenesis ($P = 1.21 \times 10^{-8}$) (Supplemental Figure 11C). In addition, we identified 3026 upregulated genes and 1142 downregulated genes in *rps2a2b-1* compared with Col-0 (Supplemental Figure 11B). The upregulated genes in *atprmt3-2* and *rps2a2b-1* showed significant overlap ($P < 10^{-100}$) (Figure 4A), and GO analysis revealed that the 1587 overlapping upregulated genes were strongly enriched in genes related to ribosome functions such as translation, peptide biosynthetic process, ribosome biogenesis, ribonucleoprotein

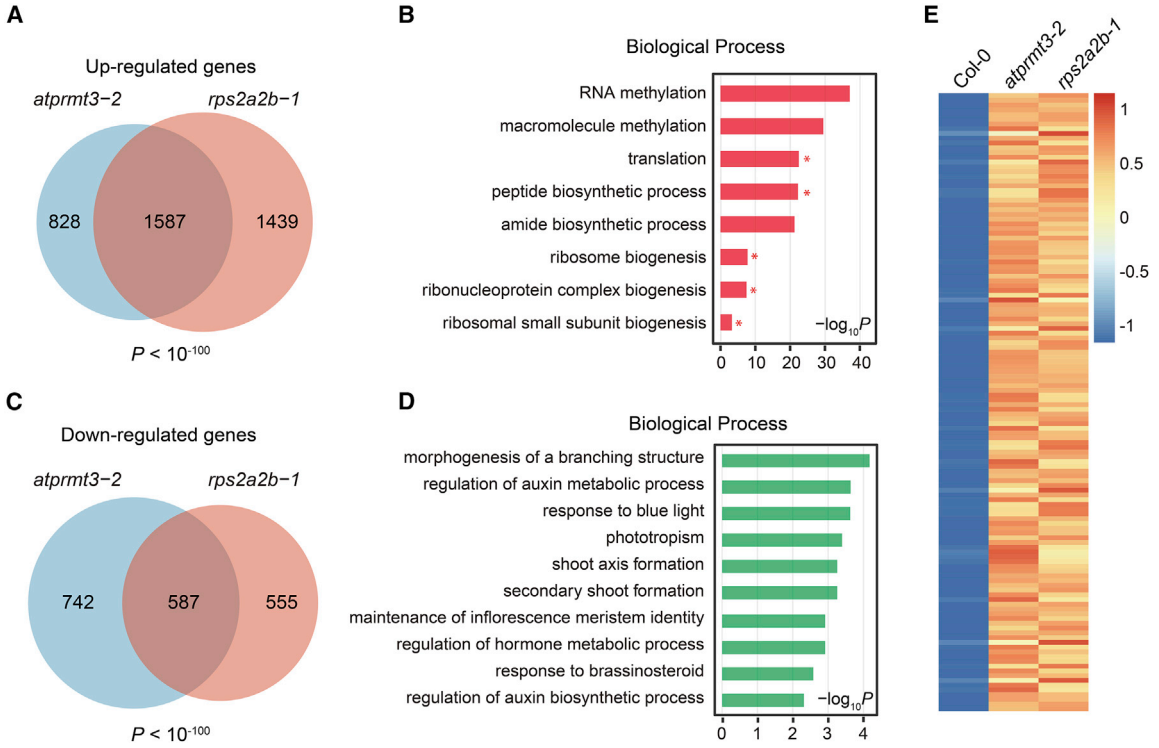

Figure 4. The Expression of Ribosome Biogenesis Factors Is Elevated in *atprmt3* Mutants.

(A and C) VENN diagram shows the upregulated genes **(A)** and downregulated genes **(C)** that overlap between the *atprmt3-2* and *rps2a2b-1* mutants. The statistical significance was determined by hypergeometric test.

(B and D) Gene Ontology analysis (Biological Process) of overlapping genes upregulated **(B)** and downregulated **(D)** in both the *atprmt3-2* and *rps2a2b-1* mutants.

(E) Heatmap of the overlapping upregulated genes enriched in ribosome-related functional categories, shown in **(B)** with asterisks. Color bar indicates the *Z*score.

complex biogenesis, and ribosomal small subunit biogenesis (Figure 4B and 4E), implying that RPS2B and AtPRMT3 have redundant functions in ribosome biogenesis. The downregulated genes in *atprmt3-2* and *rps2a2b-1* also showed significant overlap ($P < 10^{-100}$) (Figure 4C), and GO analysis revealed that the 587 overlapping downregulated genes were involved in many biological process (Figure 4D).

The U3 snoRNP contains the U3 snoRNA and core proteins, including Nucleolar protein 1 (NOP1)/FIBRILLARIN (FIB), NOP56, NOP58, Small nuclear protein 13 (Snu13), and RRP9 (Watkins and Bohnsack, 2012). Notably, genes related to the U3 snoRNP were upregulated in both the *atprmt3-2* and *rps2a2b-1* mutants (Supplemental Figure 11D and 11E), as further validated by quantitative RT–PCR (Supplemental Figure 11F). Consistent with their mRNA levels, the protein levels of FIB and NOP56 were upregulated in *atprmt3-2* and *rps2a2b-1* (Supplemental Figure 11H), reflecting the overaccumulation of the U3 snoRNP core proteins in both mutants. Moreover, snoRNAs such as U3 and snoR30 also overaccumulated in the *atprmt3-2* and *rps2a2b-1* mutants, consistent with the aberrant pre-rRNA processing in these mutants (Supplemental Figure 11G).

Disruption of *AtPRMT3* Resulted in Enlarged Nucleoli

The nucleolus, a major cellular compartment for ribosome biogenesis, is a membrane-less dynamic structure with changing size, shape, and position in the nucleus (Shaw and Brown, 2012). The nucleolus encapsulates various ribonucleoproteins and RNAs and can achieve self-organization or self-assembly, potentially through liquid–liquid phase separation (Sawyer et al., 2019; Yao et al., 2019). Aberrant ribosome biogenesis is usually correlated with disorganization of the nucleolus and results in nucleolar stress, which is often manifested by altered size of the nucleolus in ribosome-related mutants. For example, the nucleolus is enlarged in the *apum23* (Abbasi et al., 2010) and *rid2* (Ohbayashi et al., 2011) mutants, and smaller in the *apum24* mutant after sugar treatment (Maekawa et al., 2017).

To determine whether the state of nucleolus was affected by the absence of AtPRMT3, we visualized nucleoli in Col-0 and *atprmt3-2* using GFP-FIB1 and measured the area of the nucleolus indicated by GFP-FIB1 fluorescence relative to that of the nucleus indicated by 4′,6-diamidino-2-phenylindole (DAPI) staining (Figure 5A). Notably, *atprmt3-2* plants had a higher frequency of large nucleoli compared with Col-0 (Figure 5B), and we also found that the nucleoli of *rps2a2b-1* were enlarged, similar to those of *atprmt3-2* (Supplemental Figure 12), suggesting that nucleolar stress occurred when either AtPRMT3 or RPS2A2B was disrupted.

Enhanced Association between RPS2B and Pre-rRNA in *atprmt3* Mutants

The pre-rRNA processing defects of the *rps2a2b-1* mutant were first apparent in the primary transcripts of 33S(P′) and 32S in the

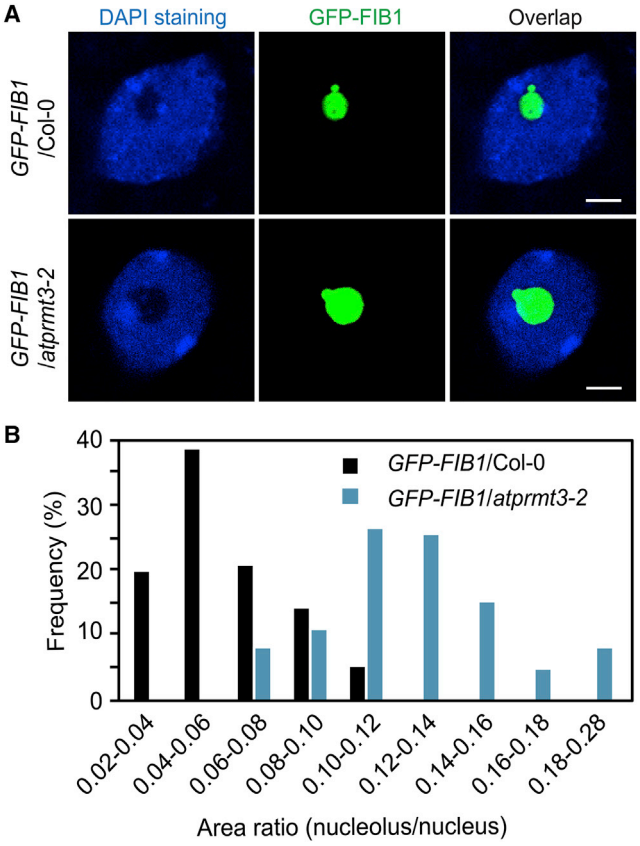

Figure 5. Disruption of AtPRMT3 Results in Enlarged Nucleoli.
(A) The nucleolus is enlarged in *atprmt3-2* mutants. The first pair of true leaves of 28-day-old seedlings of *GFP-FIB1*/Col-0 and *GFP-FIB1/atprmt3-2* were fixed in formaldehyde and stained with DAPI, and the nuclei were photographed by confocal microscopy. The nucleolus and nucleus are marked by GFP-FIB1 fluorescence in green and DAPI staining of DNA in blue, respectively. Scale bar, 2 μm.
(B) Quantitative measurement of area ratio (nucleolus/nucleus). Black and blue bars indicate *GFP-FIB1*/Col-0 and *GFP-FIB1/atprmt3-2*, respectively. In total, 90 and 98 nuclei from *GFP-FIB1*/Col-0 and *GFP-FIB1/atprmt3-2*, respectively, were recorded for measurement.

nucleolus, indicating the important function of RPS2B in the early stages of rRNA biogenesis. Indeed, subcellular fractionation assays supported the nuclear localization of RPS2B-YFP (Supplemental Figure 13A). Moreover, immunofluorescence microscopy of *RPS2B-YFP*/Col-0 plants further revealed that RPS2B-YFP can be localized in both the nucleoplasm and nucleolus (Supplemental Figure 13B), where ribosome biogenesis actively occurs in living cells. We further performed an immunofluorescence assay using the nuclei of Col-0 and found endogenous nuclear RPS2A2B to be distributed in both the nucleoplasm and nucleolus (Supplemental Figure 14). This is consistent with published data in which RPS2 proteins were identified in the nucleolus proteomes from plant cell culture (Pendle et al., 2005; Palm et al., 2016) and plants (Montacie et al., 2017). Evidence indicates that RPS2B participates in ribosome biogenesis at a relatively early stage beginning in the nucleolus.

To determine whether RPS2B regulates the processing step by binding to pre-rRNAs directly, we performed RIP experiments using GFP-Trap and the nuclear fractions of Col-0, *RPS2B-YFP*/Col-0, and *RPS2B-YFP/atprmt3-2* seedlings. We found that the pre-rRNA fragments were specifically enriched in samples with *RPS2B-YFP* but not in the wild-type Col-0 control. U5 small nuclear RNA (snRNA), used as a negative control, did not co-purify with RPS2B-YFP (Figure 6A). These results suggest that RPS2B binds to pre-rRNAs *in vivo*. Intriguingly, we found that the signal enriched by RPS2B-YFP was higher in *atprmt3-2* mutants than in Col-0 (Figure 6A), indicating an enhanced association between RPS2B and pre-rRNA in *atprmt3-2* mutants.

Retarded Assembly/Disassembly of the 90S/SSU Processome in *atprmt3* Mutants

Ribosome biogenesis is a complicated and highly orchestrated process requiring numerous assembly factors as well as ribosomal proteins (Henras et al., 2008; Lafontaine, 2015). Here, enhanced interaction between RPS2B and pre-rRNAs in the *atprmt3* mutant inspired us to compare the functional RPS2B-associated pre-ribosome complex in Col-0 and *atprmt3-2*. We first immunoprecipitated RPS2B-YFP proteins and their associated complexes from the nuclear extracts of *RPS2B-YFP*/Col-0 and *RPS2B-YFP/atprmt3-2* seedlings, with wild-type Col-0 as a negative control (Supplemental Figure 13C). RPS2B-YFP-associated proteins were characterized by LC–MS/MS analysis, using spectrum counts to quantify protein abundance. We normalized the counts to those of RPS2B to estimate the relative abundance of proteins associated with RPS2B in different samples. GO analysis using Metascape revealed that these RPS2B-associated proteins mainly function in ribosome biogenesis (Supplemental Figure 13D) (Zhou et al., 2019).

Among the RPS2B-associated proteins, intriguingly, we identified a large set of *Arabidopsis* homologs of assembly factors in yeast that comprise the 90S/SSU processome (Figure 6B [upper] and Supplemental Table 4). The 90S/SSU processome contains the 5′ ETS particle, which is an early assembly intermediate formed on the 5′ ETS that includes U 3 PROTEIN A (UTPA), UTPB, UTPC, U3 snoRNP, the M PHASE PHOSPHOPROTEIN 10 (MPP10) complex, and other assembly factors that join the complex sequentially (Barandun et al., 2018; Klinge and Woolford, 2018). Extensive studies have revealed that these factors assemble in a stepwise and dynamic manner (Chaker-Margot et al., 2015; Zhang et al., 2016). Compared with Col-0, the *atprmt3* mutants showed more normalized spectral counts for the 90S/SSU processome components, including UTPA (SWA1/UTP15 and UTP4), UTPB (UTP6, PWP2), DOM34 INTERACTING PROTEIN 2 (DIP2/UTP12), U3 snoRNP (FIB1, FIB2, NOP56, NOP58, and RRP9/YAO), and MPP10 (IMP4), as well as some complexes including Nucleolin, H/ACA snoRNP, UTPC, and other assembly factors (Figure 6B, upper). Enhanced association between RPS2B and the 90S/SSU processome in the *atprmt3* mutant suggests that AtPRMT3 functions as an important ribosome biogenesis factor in the dynamic assembly of the 90S/SSU processome. To validate the RPS2B interactome results, we immunoblotted coIP products of *RPS2B-YFP* from nuclear extracts with antibodies against U3 snoRNP core proteins, such as FIB and NOP56. Consistent with the MS results, the association between RPS2B and snoRNP increased in *atprmt3-2* mutants (Figure 6C).

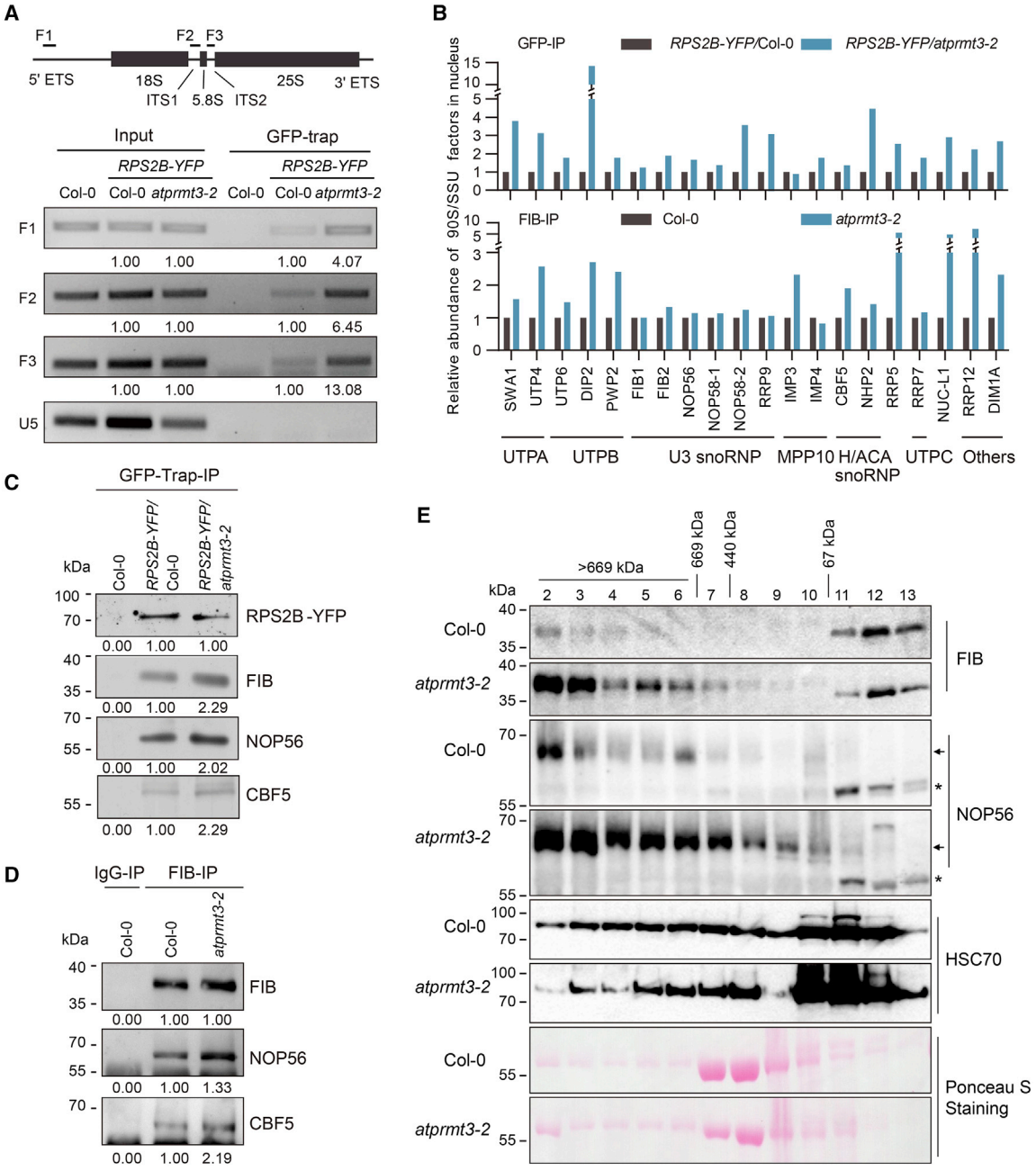

Figure 6. Assembly/Disassembly of the Pre-rRNA Processome Is Retarded in *atprmt3* Mutants.

(A) Enhanced association between RPS2B and pre-rRNAs in the *atprmt3-2* mutant. The upper diagram shows the locations of specific fragments (F1, F2, and F3) that were amplified by PCR with specific primers. RIP assays were performed with Col-0, *RPS2B-YFP*/Col-0, and *RPS2B-YFP*/*atprmt3-2* seedlings, and 1% of total RNA was used as input. U5 snRNA was the negative control. For quantification, each band was first normalized to its respective input, after which the quantity of *atprmt3-2* was normalized to that of Col-0.

(B) The associations between 90S/SSU and RPS2B (and FIB) were enhanced in the *atprmt3-2* mutant. In the top panel, nuclear extracts from *RPS2B-YFP*/Col-0 and *RPS2B-YFP*/*atprmt3-2* seedlings were immunoprecipitated with GFP-Trap; in the bottom panel, nuclear extracts from Col-0 and *atprmt3-2* were immunoprecipitated with anti-FIB. The associated proteins were identified by LC–MS/MS. The relative abundance of 90S/SSU processome factors was determined by calculating the ratio of spectral counts between *atprmt3-2* and Col-0.

(C) RPS2B-YFP-associated proteins were validated by coIP assay in Col-0, *RPS2B-YFP*/Col-0, and *RPS2B-YFP*/*atprmt3-2*. RPS2B-YFP and associated proteins were immunoprecipitated with GFP-Trap and immunoblotted with anti-NOP56 and anti-CBF5 antibodies. IP with GFP-Trap in Col-0 was the negative control. The relative abundances of RPS2B-GFP, FIB, NOP56, and CBF5 are shown below each panel.

(D) FIB-associated proteins were validated by coIP assay in Col-0 and *atprmt3-2*. FIB and associated proteins were immunoprecipitated by anti-FIB antibody and immunoblotting was performed with anti-NOP56 and anti-CBF5 antibodies. The IgG-IP in Col-0 was the negative control. The relative abundances of FIB1, NOP56, and CBF5 are shown below each panel.

(legend continued on next page)

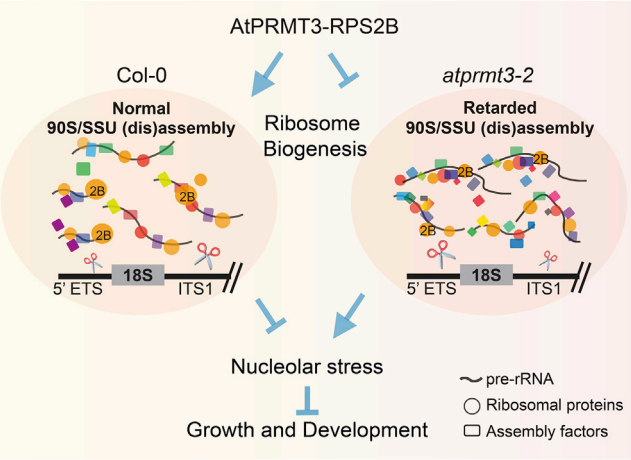

Figure 7. A Working Model Deciphering How the AtPRMT3–RPS2B Interaction Functions in Pre-ribosome Assembly and Nucleolar Stress.

In the wild type, AtPRMT3–RPS2B interaction may maintain functional or sufficient levels of RPS2B, together with other ribosomal proteins and multiple assembly factors, to promote ribosome assembly at the early stages of ribosome biogenesis in the nucleolus. When the interaction disappears, as occurs when AtPRMT3 is disrupted in *atprmt3-2*, RPS2B in the nucleus may be nonfunctional or present at insufficient levels, resulting in delayed assembly/disassembly of 90S/SSU processome, which exhibits higher association with RPS2B and many assembly factors. Aberrant ribosome biogenesis in *atprmt3-2* further triggers nucleolar stress, resulting in an enlarged nucleolus, which ultimately affects normal cellular function, plant growth, and development.

To further verify the state of the 90S/SSU processome in *atprmt3* mutants, we performed immunoprecipitation coupled with MS (IP–MS) using antibodies against FIB to identify and compare the FIB-associated components in Col-0 and *atprmt3-2*. Consistent with the RPS2B IP–MS results, the interactions between FIB and the 90S/SSU processome were also enhanced in the *atprmt3-2* mutant (Figure 6B, lower). The enhanced interactions between FIB and NOP56 as well as H/ACA ribonucleoprotein complex subunit CBF5 were then further validated by coIP (Figure 6D). Moreover, gel-filtration analysis revealed that more FIB and NOP56 were distributed in the high-molecular-weight fractions in *atprmt3-2* than in Col-0, implying that the core complex of snoRNP (FIB and NOP56) was retained in the larger complex (Figure 6E). These results suggest that AtPRMT3 promotes the dynamic assembly/disassembly of the 90S/SSU processome at the early pre-rRNA processing stages to regulate ribosome biogenesis.

DISCUSSION

Previously we showed that AtPRMT3 is essential for proper pre-rRNA processing (Hang et al., 2014), but how AtPRMT3 functions in this pathway remains unclear. Here we revealed that AtPRMT3–RPS2B interaction in *Arabidopsis* promotes ribosome biogenesis by fine-tuning the dynamic assembly/disassembly of the 90S/SSU processome in the nucleus, thereby repressing nucleolar stress during plant growth and development.

PRMTs usually catalyze arginine methylation of different substrates to regulate diverse biological processes (Bedford and Clarke, 2009; Ahmad and Cao, 2012). However, in this study we identified an intragenic mutant and demonstrated that AtPRMT3 functions through protein–protein interaction rather than its enzymatic activity, similar to PRMT3 in yeast (Perreault et al., 2009). The PRMT3–RPS2 interaction is conserved in unicellular fission yeast (Bachand and Silver, 2004) and multicellular organisms, such as mouse (Swiercz et al., 2007) and human cells (Swiercz et al., 2005). However, its underlying biological function remains elusive. In this work, we found that RPS2B physically interacts with AtPRMT3 in *Arabidopsis* and that mutants of these genes share similar biological and molecular defects, indicating that AtPRMT3 and RPS2B are involved in the same pathway. Moreover, the PRMT3–RPS2 interaction *in vivo* involves only the N-terminal C2H2-zinc-finger domain of AtPRMT3, and this domain was sufficient for AtPRMT3 function. Earlier work in human cells suggested that PRMT3 may protect RPS2 from ubiquitin-mediated proteolysis (Choi et al., 2008). RPS2B has a highly basic N-terminal RGG/RG domain; these RNA binding domains are found in many proteins involved in phase separation (Chong et al., 2018). Due to the highly conserved function of PRMT3, we hypothesize that AtPRMT3 might function as a chaperone to prevent non-specific interactions or aggregation and to help RPS2 efficiently incorporate into the pre-ribosome, as shown for the chaperones in yeast (Pillet et al., 2017).

Alternative pre-rRNA processing pathways differ in the order of 5′ ETS removal and ITS1 cleavage (Hang et al., 2014; Weis et al., 2015a, 2015b; Tomecki et al., 2017; Hang et al., 2018; Saez-Vásquez and Delseny, 2019), and these processing pathways are dependent on the stepwise and dynamic assembly of the pre-ribosomal complexes (Klinge and Woolford, 2018; Cheng et al., 2020; Du et al., 2020). Here we characterized a large set of *Arabidopsis* homologs for 90S/SSU processome components, including UTPA, UTPB, U3 snoRNP, MPP10, and UTPC. These proteins co-purified with FIB and RPS2B in the nucleus, demonstrating the existence of the 90S/SSU complex in higher plants (Saez-Vásquez and Delseny, 2019). We propose a working model in which AtPRMT3–RPS2B interaction is essential for proper ribosome biogenesis, especially the dynamic assembly of the 90S/SSU processome in the nucleolus, to promote cellular function, plant growth, and development (Figure 7). AtPRMT3 may regulate the amount of RPS2B available to incorporate into the pre-ribosome to promote dynamic assembly/disassembly of the 90S/SSU processome. Disruption of the AtPRMT3–RPS2B interaction may delay the dynamic assembly/disassembly of 90S/SSU processome on 35S(P) transcripts and affect the downstream balance of "5′ ETS-first" and "ITS1-first" processing, in which removal of the 5′ ETS occurs before the cleavage in the ITS1. Aberrant ribosome

(E) Gel-filtration patterns of FIB and NOP56 in Col-0 and *atprmt3-2*. Total protein lysates from Col-0 and *atprmt3-2* were fractioned by gel filtration. Arrows indicate the bands of NOP56 in each group. Asterisks represent the unspecific signals. The patterns of HSC70 and Ponceau S staining represent the negative controls.

biogenesis further leads to nucleolar stress, resulting in aberrant cellular function and finally causing growth and developmental defects (Figure 7).

Defects in ribosome biogenesis are usually accompanied by changes in the composition and organization of the nucleolus, resulting in nucleolar stress (Matos-Perdomo and Machin, 2019). Mechanisms underlying nucleolar stress are complex. In animals, nucleolus stress can trigger the binding of specific ribosomal proteins to the ubiquitin E3 ligase MDM2, which inhibits MDM2-mediated p53 ubiquitination, leading to the activation of p53 (Zhang and Lu, 2009). Recent work has reported that ANAC082 might serve as a nucleolar stress mediator in *Arabidopsis* (Ohbayashi et al., 2017), while the detailed mechanism remains elusive in plants. It will be informative to determine whether and how ANAC082 is activated by disruption of the AtPRMT3–RPS2B interaction and mediates the nucleolar stress responses, which may account for the growth and developmental defects of *atprmt3-2* and *rps2a2b-1*. In addition, the membrane-less nucleolus exhibits liquid–liquid phase separation characteristics (Sawyer et al., 2019) and serves as a central compartment sensing stress and coordinating stress responses (Zhang and Lu, 2009; Boulon et al., 2010). Nucleolar stress can also be induced by environmental stresses such as extreme temperature (Boulon et al., 2010). Interestingly, extreme temperatures such as cold or heat stress can severely affect ribosome biogenesis in rice, thereby restricting plant growth and product yield (Wang et al., 2016; Hang et al., 2018). However, it is still unknown whether the plant nucleolus acts as a temperature sensor to quickly adjust cellular ribosome biogenesis and metabolism for better acclimation to ambient temperature fluctuations. Since AtPRMT3–RPS2B interaction promotes ribosome biogenesis and represses nucleolar stress, it will be intriguing to determine the functions of AtPRMT3 and RPS2B in extreme temperature responses in the future.

METHODS

Plant Materials

The *atprmt3*-2 (WISCDSLOX391A01) mutant was characterized previously (Hang et al., 2014). The *rps2a-1* (SALKseq_48220.1) and *rps2c-1* (SALK_020959C) mutants were obtained from the Arabidopsis Biological Resource Center. The *rps2a2b-1* mutant was created by CRISPR/Cas9 editing (Wang et al., 2015). The *rps2d-1* and *rps2d-2* mutants were also created by CRISPR/Cas9 editing (Tsutsui and Higashiyama, 2017).

EMS Mutagenesis, Genomic DNA Sequencing, and Data Analysis

atprmt3-2 seeds (0.1 g) were mutagenized with 0.3% EMS and 0.01% Tween-20 for 15 h and then planted on soil. M2 seeds were collected from individual M1 plants. The M2 generation was screened for rescue of the *atprmt3* mutant phenotypes. The suppressors were backcrossed to *atprmt3-2* at least three times before further genetic analysis. Seedlings showing wild-type and mutant phenotypes were pooled separately in the F2 generation for whole-genome sequencing using the Illumina NovaSeq6000 platform, which was performed by Berry Genomics. The reads were trimmed using Trimmomatic (Bolger et al., 2014) and mapped to the reference *Arabidopsis thaliana* genome (TAIR10) using BWA-MEM (Li and Durbin, 2009; Li, 2013). Alignments were then sorted with samtools (Li et al., 2009) and duplicates were marked with PicardTools (http://broadinstitute.github.io/picard). SNPs called with samtools/bcftools were then filtered using mapping quality ≥30 as a threshold (Li, 2011). The SNP index for each allele at segregating bi-allelic SNPs in 100-kb sliding windows (by 10 kb) was summed for the various sequencing pools and allele frequencies calculated. Finally, the difference in allele frequency (SNP index) between the mutant pool and wild-type pool was calculated for all pairwise comparisons and plotted across the five chromosomes.

Northern Blot Analysis

Northern blotting was conducted as previously described (Hang et al., 2014). The probes in this study are listed in Supplemental Table 2 or were previously described (Hang et al., 2014).

Subcellular Fractionation

Subcellular fractionation was conducted as previously described with minor modification (Hang et al., 2014). In brief, 1-g seedlings were ground thoroughly in 2 ml of Honda buffer (25 mM Tris–HCl, [pH 7.4], 2.5% Ficoll 400, 5% dextran T40, 0.4 M sucrose, 10 mM $MgCl_2$, 1 mM dithiothreitol [DTT], and protease inhibitors) at 4°C, after which the suspension was filtered through 60-μm mesh nylon netting. Triton X-100 was added to a final concentration of 0.5% and the sample was incubated on ice for 30 min, then centrifuged at 1500 *g* for 5 min. The supernatant was then centrifuged at 13,000 *g* for 5 min and kept as the cytoplasmic fraction. The pellet was resuspended in suspension buffer (10 mM Tris–HCl [pH 8.0], 0.25 M sucrose, 10 mM $MgCl_2$, 1% Triton X-100, and protease inhibitors) and centrifuged at 1500 *g* for 5 min, and this step was repeated two or three times to remove the green debris until the pellet turned white. Finally, the pellet was suspended in nuclear lysis buffer (50 mM Tris–HCl [pH 8.0], 10 mM EDTA [pH 8.0], 1% SDS, 1 mM DTT, and protease inhibitors) and gently mixed for 1 h at 4°C, then sonicated to release more nuclear proteins. The nuclear fraction was centrifuged at 13 000 *g* for 5 min to remove debris.

Circular RT–PCR Assay

The circular RT–PCR assay was performed as described previously (Hang et al., 2014, 2015) with a minor modification in that SuperScript II reverse transcriptase (Invitrogen, 18064022) was used for the reverse transcription step.

Generation of Complementation Lines *RPS2A$_{pro}$::RPS2A-GFP-HIS*, *RPS2B$_{pro}$::RPS2B-GFP-HIS*, and *RPS2B$_{pro}$::RPS2A-GFP-HIS* in *rps2a2b-1*

The genomic fragments of *RPS2A* (905 bp upstream of the start codon and the 968-bp genomic region without the stop codon) and *RPS2B* (717 bp upstream of the start codon and the 1196-bp genomic region without the stop codon) were amplified by primers HX1739/HX1740 and HX1735/HX1705, respectively. Both fragments were cloned into the pENTR-D-TOPO vector (Life Technologies, K2400-20) to generate XF2957 (TOPO-*RPS2A$_{pro}$*::*RPS2A*) and XF2958 (TOPO-*RPS2B$_{pro}$*::*RPS2B*), respectively. After digestion with the restriction enzyme *Mlu*I (NEB, R0198S), fragments containing *RPS2A* and *RPS2B* were cloned into the destination vector *pMDC107* using Gateway LR Clonase II (Life Technologies, 11791-100) to generate DNA constructs XF2066 (*RPS2A$_{pro}$*::*RPS2A-GFP-6×HIS*) and XF2967 (*RPS2B$_{pro}$*::*RPS2B-GFP-6×HIS*), respectively. Similarly, the gene body of *RPS2A* with the promoter of *RPS2B* was cloned in *pMDC107* and named *RPS2B$_{pro}$*::*RPS2A-GFP-6×HIS*. The constructs were then introduced into the *Agrobacterium tumefaciens* strain EHA105 and transformed into the *rps2a2b-1* mutant to generate the *RPS2A-GFP*, *RPS2B-GFP*, and *RPS2B$_{pro}$*::*RPS2A-GFP* complementation lines. All primers are listed in Supplemental Table 2.

Generation of *35S$_{pro}$::RPS2B-YFP-HA* in Col-0 and *atprmt3-2* Mutants

The cDNA fragment of *RPS2B* was amplified by primers HX4160/HX4161 and cloned into *pEASY-T1* (Transgen Biotech, CT101-01) to generate the construct XF2935. Using XF2935 as the template, the full-length coding

sequence (CDS) of *RPS2B* was amplified by primers HX1703/HX1705 and subcloned into the target vector *pEG101* by Gateway cloning (Earley et al., 2006) to generate the construct XF2967 (*35S$_{pro}$::RPS2B-YFP-HA*). The construct was introduced into *A. tumefaciens* strain EHA105 and then into Col-0 to generate *RPS2B-YFP*/Col-0. A transgenic plant was crossed with *atprmt3-2*, and progeny were screened to identify homozygous *RPS2B-YFP/atprmt3-2*. All primers are presented in Supplemental Table 2.

Generation of Transgenic Lines of *AtPRMT3$_{pro}$::AtPRMT3^{E374Q}-GFP-HIS*, *UBQ10$_{pro}$::AtPRMT3^{WT}-HA*, and *UBQ10$_{pro}$::AtPRMT3^{N}-HA* in *atprmt3-2*

The point mutation construct XF2891 (*AtPRMT3$_{pro}$::AtPRMT3^{E374Q}-GFP-HIS*) was created using primers HX2708/HX2709 to perform site-directed mutagenesis of XF1630 (*AtPRMT3$_{pro}$::AtPRMT3^{WT}-GFP-HIS*) (Hang et al., 2014). The CDS regions encoding full-length AtPRMT3 and its N terminus (amino acids 1–171) amplified by primers HX6075/HX6076 and HX6075/HX7568, respectively, were cloned into the XF1724 vector to generate the constructs XF3379 (*UBQ10$_{pro}$::AtPRMT3^{WT}-HA*) and XF3500 (*UBQ10$_{pro}$::AtPRMT3^{N}-HA*). These constructs were introduced into *A. tumefaciens* strain EHA105 and then into *atprmt3-2* to generate *AtPRMT3^{WT}-GFP*, *AtPRMT3^{E374Q}-GFP*, *AtPRMT3^{WT}-HA*, and *AtPRMT3^{N}-HA*. All primers are listed in Supplemental Table 2.

Proteomic Analysis

The products immunoprecipitated by the indicated antibodies were separated by SDS–PAGE, and protein bands (excluding the antibody heavy and light chains) were digested by trypsin and recovered from the gel. The samples were analyzed by LC–MS using a Nano LC–MS/MS (Dionex Ultimate 3000 RLSCnano System) interfaced with QExactive HF. The data were analyzed with MaxQuant software (1.3.0.5), using the TAIR10 database.

Phylogenetic Analysis and Sequence Alignment of RPS2 Proteins

Database searches were performed at TAIR10 (www.arabidopsis.org/Blast/index.jsp) and NCBI (www.ncbi.nlm.nih.gov). Multiple alignments of protein sequences were performed with Clustal X (Larkin et al., 2007) and alignments were manually edited with the GeneDoc program. Evolutionary analyses were conducted with the neighbor-joining method in MEGA6 (Tamura et al., 2013).

Histological Analysis of Seedlings

Histological analysis of cotyledons and the first leaves of 24-day-old seedlings was performed as described previously (Hang et al., 2014) with ClearSee solution (Kurihara et al., 2015). Images were taken with an Olympus SZX12 microscope.

Recombinant Protein Expression, *In Vitro* Methyltransferase Assay, and Pull-Down Assay

Specific CDS regions of *RPS2A*, *RPS2B*, *RPS2C*, and *RPS2D* were cloned into XF0510 to generate the constructs XF2939 (*HIS-MBP-RPS2A*), XF2942 (*HIS-MBP-RPS2B*), XF2945 (*HIS-MBP-RPS2C*), and XF2948 (*HIS-MBP-RPS2D*), respectively. XF2895 (*GST-AtPRMT3^{E374Q}*) was created by site-directed mutagenesis of XF193 (*GST-AtPRMT3*) (Hang et al., 2014) using primers HX2708/HX2709. The CDS of AtPRMT3^{N} (amino acids 1–171) was amplified using primers HX1172/HX1173 and cloned into XF760 to generate XF2901 (*GST-AtPRMT3^{N}*). Recombinant proteins were expressed in the *Escherichia coli* strain BL21 (RIL). Methyltransferase activity assays were performed as previously described (Hang et al., 2014). For *in vitro* pull-down assays, 5 μg of HIS-MBP and HIS-MBP-RPS2 proteins were first immobilized to Ni-charged Profinity IMAC Resin as the bait proteins, followed by blocking with 5% BSA at 4°C for 2 h in BW buffer (50 mM Tris–HCl [pH 8.0], 300 mM NaCl, and 0.1% [m/v] CA-630). Each immobilized bait protein was then incubated with 5 μg of GST-AtPRMT3, GST-AtPRMT3^{N}, or GST (as prey) at room temperature for 30 min, before finally being washed five times with BW buffer. Immunoblotting was performed with anti-GST antiserum.

Antibodies Used in Immunoblotting

GST-RPS2B-N (amino acids 1–50) and HIS-MBP-RPS2B-C (amino acids 51–284) were used as antigens to produce RPS2B-N mouse antibody and RPS2B-C rabbit antibody, respectively. HIS-MBP-NOP56 (NP_176007.1) and HIS-SUMO-CBF5/NAP57 (NP_191274.1) were used to generate CBF5 and NOP56 mouse antiserum, respectively. Rabbit antibodies of FIB (NP_568772.3) were made at Abclonal, using amino acids 51–308 of FIB1 as the antigen. The specificities of the NOP56 and FIB antibodies were validated as shown in Supplemental Figure 15. The commercial antibodies used include anti-histone H3 (Abcam, ab1791), anti-PEPC (Agrisera, AS09458), and anti-HSC70 (Enzo, ADI-SPA-818-D).

Subcellular Localization of RPS2B and Nucleolus/Nucleus Area Measurement

For the *in vivo* subcellular localization assay of RPS2B-YFP in Supplemental Figure 13B, 10-day-old transgenic seedlings of *35S$_{pro}$::RPS2B-YFP-HA* were fixed in 4% paraformaldehyde (Thermo Scientific, 28908) in 1× PBS buffer. Nuclei were then isolated and immunofluorescence imaging performed as described previously (Bey et al., 2018). The primary antibody against FIB and the secondary donkey anti-rabbit immunoglobulin G (IgG) (H + L) (Highly Cross-Adsorbed Secondary Antibody, Alexa Fluor 555, Thermo Fisher A-31572) were used. For the subcellular localization assay of endogenous RPS2A2B in Supplemental Figure 14B, 12-day-old seedlings of Col-0 were fixed, and nuclei were isolated for immunofluorescence imaging as described above with rabbit anti-RPS2B-C. For the area measurements of nucleoli and nuclei in Figure 5A, *GFP-FIB1*/Col-0 and *GFP-FIB1/atprmt3-2* lines containing the same transgene, CXF0332 (*35S$_{pro}$::GFP-FIB1*), were used. For the area measurements of nucleoli and nuclei in Supplemental Figure 12A, Col-0, *atprmt3-2*, and *rps2a2b-1* were used. The first pair of true leaves of 28-day-old seedlings were fixed in 4% paraformaldehyde (Thermo Scientific, 28908) in 1× PBS buffer. DAPI was added at a final concentration of 1 μg/ml to stain for DNA as described previously (Abbasi et al., 2010). Images were taken with a Zeiss LSM510 inverted confocal microscope equipped with a Plan-Apochromat 100×/1.4 oil DIC objective, a Zeiss Axio Observer Z1 lens, and an Axiocam 506 mono CCD camera (Carl Zeiss, Thornwood, NY). The nucleolar and nuclear areas were measured using ImageJ software.

Embryo Microscopy

The embryos were incubated in Hoyer's solution (chloral hydrate/distilled water/glycerol = 8:3:1, m/v/v) for 45 min at 4°C, then incubated at room temperature until the embryos were clear. The embryos were photographed with a BX51 microscope (Olympus) in the differential interference contrast mode.

Bimolecular Fluorescence Complementation

The CDSs of *AtPRMT3* (amplified by primers H538 and H540) and *RPS2B* (amplified using primers H541 and H542) were cloned into the pXY106 and pXY104 vectors (Zhang et al., 2015, 2020), respectively. Constructs were transformed into *Agrobacterium* GV3101. Bacteria transformed with different protein constructs were co-infiltrated into the leaves of 4-week-old tobacco (*Nicotiana benthamiana*). After 36–48 h, YFP signals were analyzed by an Olympus BX53 Digital Fluorescence Microscope.

RIP RT–PCR

Two grams of 12-day-old seedlings were incubated in ice-cold 1× PBS buffer and crosslinked twice at 800 mJ/cm^2 in a Hoefer UVC 500 ML Ultraviolet Crosslinker (GE). The nuclei were extracted as previously described (Bowler et al., 2004). The RIP experiment was performed as

described by Chen et al. (2018). GFP-Trap beads (ChromoTek, gtma-10) were used for IP. Finally, the immunoprecipitated RNA was reverse transcribed with random primers (TransGen, AH301-02). Gene-specific primers (Supplemental Table 2) were used for RT–PCR to detect the target transcripts.

RNA Sequencing and Analysis

Total RNA from 12-day-old seedlings was subjected to poly(A) selection, and strand-specific RNA-sequencing libraries were constructed using the deoxyuridine triposphate method (Levin et al., 2010). All clean reads were aligned and normalized as previously described (Zhao et al., 2019). Genes with FDR (false discovery rate) values less than 0.05 and fold change over 1.5 were identified as differentially expressed genes using edgeR (Robinson et al., 2010). GO was analyzed using GOstats (Falcon and Gentleman, 2006), and the *P*-value cutoff was set to 0.05.

ACCESSION NUMBERS

The RNA-sequencing dataset was deposited in the National Center for Biotechnology Information Gene Expression Omnibus under the accession number GEO: GSE140318 (https://www.ncbi.nlm.nih.gov/geo/query/acc.cgi?acc=GSE140318). The DNA-resequencing dataset was deposited in the Sequence Read Archive database under the accession number SRA:PRJNA614590 (https://www.ncbi.nlm.nih.gov/bioproject/PRJNA614590).

SUPPLEMENTAL INFORMATION

Supplemental Information can be found online at *Molecular Plant Online*.

FUNDING

This work was supported by grants from the National Natural Science Foundation of China (31788103 and 91540203 to X. Cao, 31770874 to C.L., 31900932 to R.H., and 31701096 to J.S.), China; the Strategic Priority Research Program of Chinese Academy of Sciences (XDB27030201 to X. Cao), China; the Key Research Program of Frontier Sciences of Chinese Academy of Sciences (QYZDY-SSW-SMC022 to X. Cao), China; and the State Key Laboratory of Plant Genomics, China.

AUTHOR CONTRIBUTIONS

R.H., Z.W., C.L., and X. Cao conceived and designed the study. R.H. and Z.W. performed most of the experiments. J.S. analyzed the RNA-sequencing data. C.Y. and L.L. interpreted the DNA-resequencing data. R.H., Z.W., C.Y., L.L., J.S., B.M., X. Chen, C.L., and X. Cao interpreted the data. R.H., Z.W., and X. Cao wrote the paper. All authors commented on the manuscript.

ACKNOWLEDGMENTS

We thank Dr. Haiyan Zheng, Rutgers University, for conducting the mass spectrometry analysis. We thank Dr. Qijun Chen, China Agricultural University, for providing the CRISPR/Cas9 vector. We thank Huankai Zhang and Dr. Xianshen Zhang, Shandong Agricultural University, for assistance in the microscopy of embryonic development. We thank Dr. Bailong Zhang and Dr. Meng Chen, University of California, Riverside, for assistance in the immunofluorescence assays. We thank Dr. Yong Zhang, University of California, Riverside, for sharing the CBF5 antiserum. We thank the Arabidopsis Biological Resource Center for providing T-DNA insertion lines. No conflict of interest declared.

Received: April 3, 2020
Revised: August 17, 2020
Accepted: October 13, 2020
Published: October 14, 2020

REFERENCES

Abbasi, N., Kim, H.B., Park, N.I., Kim, H.S., Kim, Y.K., Park, Y.I., and Choi, S.B. (2010). APUM23, a nucleolar Puf domain protein, is involved in pre-ribosomal RNA processing and normal growth patterning in *Arabidopsis*. Plant J. **64**:960–976.

Ahmad, A., and Cao, X. (2012). Plant PRMTs broaden the scope of arginine methylation. J. Genet. Genomics **39**:195–208.

Bachand, F.O., and Silver, P.A. (2004). PRMT3 is a ribosomal protein methyltransferase that affects the cellular levels of ribosomal subunits. EMBO J. **23**:2641–2650.

Ban, N., Beckmann, R., Cate, J.H., Dinman, J.D., Dragon, F., Ellis, S.R., Lafontaine, D.L., Lindahl, L., Liljas, A., Lipton, J.M., et al. (2014). A new system for naming ribosomal proteins. Curr. Opin. Struct. Biol. **24**:165–169.

Barandun, J., Hunziker, M., and Klinge, S. (2018). Assembly and structure of the SSU processome—a nucleolar precursor of the small ribosomal subunit. Curr. Opin. Struc Biol. **49**:85–93.

Bedford, M.T., and Clarke, S.G. (2009). Protein arginine methylation in mammals: who, what, and why. Mol. Cell **33**:1–13.

Bey, T.D., Koini, M., and Fransz, P. (2018). Fluorescence in situ hybridization (FISH) and immunolabeling on 3D preserved nuclei. Methods Mol. Biol. **1675**:467–480.

Bolger, A.M., Lohse, M., and Usadel, B. (2014). Trimmomatic: a flexible trimmer for Illumina sequence data. Bioinformatics **30**:2114–2120.

Boulon, S., Westman, B.J., Hutten, S., Boisvert, F.M., and Lamond, A.I. (2010). The nucleolus under stress. Mol. Cell **40**:216–227.

Bowler, C., Benvenuto, G., Laflamme, P., Molino, D., Probst, A.V., Tariq, M., and Paszkowski, J. (2004). Chromatin techniques for plant cells. Plant J. **39**:776–789.

Byrne, M.E. (2009). A role for the ribosome in development. Trends Plant Sci. **14**:512–519.

Caparros-Ruiz, D., Lahmy, S., Piersanti, S., and Echeverria, M. (1997). Two ribosomal DNA-binding factors interact with a cluster of motifs on the 59 external transcribed spacer, upstream from the primary pre-rRNA processing site in a higher plant. Eur. J. Biochem. **247**:981–989.

Chaker-Margot, M., Hunziker, M., Barandun, J., Dill, B.D., and Klinge, S. (2015). Stage-specific assembly events of the 6-MDa small-subunit processome initiate eukaryotic ribosome biogenesis. Nat. Struct. Mol. Biol. **22**:920–923.

Chen, X., Ding, A.B., and Zhong, X. (2020). Functions and mechanisms of plant histone deacetylases. Sci. China Life Sci. **63**:206–216.

Chen, X., Lu, L., Qian, S., Scalf, M., Smith, L.M., and Zhong, X. (2018). Canonical and non-canonical actions of *Arabidopsis* histone deacetylases in ribosomal RNA processing. Plant Cell **30**:134–152.

Cheng, J., Lau, B., La Venuta, G., Ameismeier, M., Berninghausen, O., Hurt, E., and Beckmann, R. (2020). 90S pre-ribosome transformation into the primordial 40S subunit. Science **369**:1470–1476.

Choi, S., Jung, C.R., Kim, J.Y., and Im, D.S. (2008). PRMT3 inhibits ubiquitination of ribosomal protein S2 and together forms an active enzyme complex. Biochim. Biophys. Acta **1780**:1062–1069.

Chong, P.A., Vernon, R.M., and Forman-Kay, J.D. (2018). RGG/RG motif regions in RNA binding and phase separation. J. Mol. Biol. **430**:4650–4665.

de la Cruz, J., Karbstein, K., and Woolford, J.L., Jr. (2015). Functions of ribosomal proteins in assembly of eukaryotic ribosomes *in vivo*. Annu. Rev. Biochem. **84**:93–129.

Dragon, F., Gallagher, J.E., Compagnone-Post, P.A., Mitchell, B.M., Porwancher, K.A., Wehner, K.A., Wormsley, S., Settlage, R.E., Shabanowitz, J., Osheim, Y., et al. (2002). A large nucleolar U3 ribonucleoprotein required for 18S ribosomal RNA biogenesis. Nature **417**:967–970.

Du, Y., An, W., Zhu, X., Sun, Q., Qi, J., and Ye, K. (2020). Cryo-EM structure of 90S small ribosomal subunit precursors in transition states. Science **369**:1477–1481.

Dutca, L.M., Gallagher, J.E., and Baserga, S.J. (2011). The initial U3 snoRNA: pre-rRNA base pairing interaction required for pre-18S rRNA folding revealed by *in vivo* chemical probing. Nucleic Acids Res. **39**:5164–5180.

Earley, K.W., Haag, J.R., Pontes, O., Opper, K., Juehne, T., Song, K., and Pikaard, C.S. (2006). Gateway-compatible vectors for plant functional genomics and proteomics. Plant J. **45**:616–629.

Falcon, S., and Gentleman, R. (2006). Using GOstats to test gene lists for GO term association. Bioinformatics **23**:257–258.

Grandi, P., Rybin, V., Bassler, J., Petfalski, E., Strauss, D., Marzioch, M., Schafer, T., Kuster, B., Tschochner, H., Tollervey, D., et al. (2002). 90S pre-ribosomes include the 35S pre-rRNA, the U3 snoRNP, and 40S subunit processing factors but predominantly lack 60S synthesis factors. Mol. Cell **10**:105–115.

Hang, R., Deng, X., Liu, C., Mo, B., and Cao, X. (2015). Circular RT-PCR assay using *Arabidopsis* samples. BioProtoc **5**:e1533.

Hang, R., Wang, Z., Deng, X., Liu, C., Yan, B., Yang, C., Song, X., Mo, B., and Cao, X. (2018). Ribosomal RNA biogenesis and its response to chilling stress in *Oryza sativa*. Plant Physiol. **177**:381–397.

Hang, R., Liu, C., Ahmad, A., Zhang, Y., Lu, F., and Cao, X. (2014). *Arabidopsis* protein arginine methyltransferase 3 is required for ribosome biogenesis by affecting precursor ribosomal RNA processing. Proc. Natl. Acad. Sci. U S A **111**:16190–16195.

Henras, A.K., Soudet, J., Gerus, M., Lebaron, S., Caizergues-Ferrer, M., Mougin, A., and Henry, Y. (2008). The post-transcriptional steps of eukaryotic ribosome biogenesis. Cell. Mol. Life Sci. **65**:2334–2359.

Horiguchi, G., Molla-Morales, A., Perez-Perez, J.M., Kojima, K., Robles, P., Ponce, M.R., Micol, J.L., and Tsukaya, H. (2011). Differential contributions of ribosomal protein genes to *Arabidopsis thaliana* leaf development. Plant J. **65**:724–736.

Klinge, S., and Woolford, J.L., Jr. (2018). Ribosome assembly coming into focus. Nat. Rev. Mol. Cell Biol. **20**:116–131.

Kojima, H., Suzuki, T., Kato, T., Enomoto, K., Sato, S., Kato, T., Tabata, S., Saez-Vásquez, J., Echeverria, M., Nakagawa, T., et al. (2007). Sugar-inducible expression of the nucleolin-1 gene of *Arabidopsis thaliana* and its role in ribosome synthesis, growth and development. Plant J. **49**:1053–1063.

Kurihara, D., Mizuta, Y., Sato, Y., and Higashiyama, T. (2015). ClearSee: a rapid optical clearing reagent for whole-plant fluorescence imaging. Development **142**:4168–4179.

Lafontaine, D.L.J. (2015). Noncoding RNAs in eukaryotic ribosome biogenesis and function. Nat. Struct. Mol. Biol. **22**:11–19.

Larkin, M.A., Blackshields, G., Brown, N.P., Chenna, R., McGettigan, P.A., McWilliam, H., Valentin, F., Wallace, I.M., Wilm, A., Lopez, R., et al. (2007). Clustal W and Clustal X version 2.0. Bioinformatics **23**:2947–2948.

Levin, J.Z., Yassour, M., Adiconis, X., Nusbaum, C., Thompson, D.A., Friedman, N., Gnirke, A., and Regev, A. (2010). Comprehensive comparative analysis of strand-specific RNA sequencing methods. Nat. Methods **7**:709–715.

Li, H., Liu, N., Shi, D., Liu, J., and Yang, W. (2010). YAO is a nucleolar WD40-repeat protein critical for embryogenesis and gametogenesis in *Arabidopsis*. BMC Plant Biol. **10**:169.

Li, H. (2011). A statistical framework for SNP calling, mutation discovery, association mapping and population genetical parameter estimation from sequencing data. Bioinformatics **27**:2987–2993.

Li, H. (2013). Aligning sequence reads, clone sequences and assembly contigs with BWA-MEM. arXiv, 1303.3997.

Li, H., and Durbin, R. (2009). Fast and accurate short read alignment with Burrows-Wheeler transform. Bioinformatics **25**:1754–1760.

Li, H., Handsaker, B., Wysoker, A., Fennell, T., Ruan, J., Homer, N., Marth, G., Abecasis, G., and Durbin, R.; 1000 Genome Project Data Processing Subgroup (2009). The sequence alignment/map format and SAMtools. Bioinformatics **25**:2078–2079.

Liu, C., Lu, F., Cui, X., and Cao, X. (2010). Histone methylation in higher plants. Annu. Rev. Plant Biol. **61**:395–420.

Maekawa, S., Ishida, T., and Yanagisawa, S. (2017). Reduced expression of APUM24, encoding a novel rRNA processing factor, induces sugar-dependent nucleolar stress and altered sugar responses in *Arabidopsis thaliana*. Plant Cell **30**:209–227.

Marmier-Gourrier, N., Clery, A., Schlotter, F., Senty-Segault, V., and Branlant, C. (2011). A second base pair interaction between U3 small nucleolar RNA and the 5'-ETS region is required for early cleavage of the yeast pre-ribosomal RNA. Nucleic Acids Res. **39**:9731–9745.

Matos-Perdomo, E., and Machin, F. (2019). Nucleolar and ribosomal DNA structure under stress: yeast lessons for aging and cancer. Cells **8**:779.

Montacie, C., Durut, N., Opsomer, A., Palm, D., Comella, P., Picart, C., Carpentier, M.C., Pontvianne, F., Carapito, C., Schleiff, E., et al. (2017). Nucleolar proteome analysis and proteasomal activity assays reveal a link between nucleolus and 26S proteasome in A. Thaliana. Front. Plant Sci. **8**:1815.

Micol-Ponce, R., Sarmiento-Manus, R., Ruiz-Bayon, A., Montacie, C., Saez-Vásquez, J., and Ponce, M.R. (2018). *Arabidopsis* RIBOSOMAL RNA PROCESSING7 is required for 18S rRNA maturation. Plant Cell **30**:2855–2872.

Missbach, S., Weis, B.L., Martin, R., Simm, S., Bohnsack, M.T., and Schleiff, E. (2013). 40S ribosome biogenesis co-factors are essential for gametophyte and embryo development. PLoS One **8**:e54084.

Narla, A., and Ebert, B.L. (2010). Ribosomopathies: human disorders of ribosome dysfunction. Blood **115**:3196–3205.

Ohbayashi, I., Konishi, M., Ebine, K., and Sugiyama, M. (2011). Genetic identification of *Arabidopsis* RID2 as an essential factor involved in pre-rRNA processing. Plant J. **67**:49–60.

Ohbayashi, I., Lin, C.Y., Shinohara, N., Matsumura, Y., Machida, Y., Horiguchi, G., Tsukaya, H., and Sugiyama, M. (2017). Evidence for a role of ANAC082 as a ribosomal stress response mediator leading to growth defects and developmental alterations in *Arabidopsis*. Plant Cell **29**:2644–2660.

Ohbayashi, I., and Sugiyama, M. (2017). Plant nucleolar stress response, a new face in the NAC-dependent cellular stress responses. Front. Plant Sci. **8**:2247.

Osheim, Y.N., French, S.L., Keck, K.M., Champion, E.A., Spasov, K., Dragon, F., Baserga, S.J., and Beyer, A.L. (2004). Pre-18S ribosomal RNA is structurally compacted into the SSU processome prior to being cleaved from nascent transcripts in *Saccharomyces cerevisiae*. Mol. Cell **16**:943–954.

Palm, D., Simm, S., Darm, K., Weis, B.L., Ruprecht, M., Schleiff, E., and Scharf, C. (2016). Proteome distribution between nucleoplasm and nucleolus and its relation to ribosome biogenesis in *Arabidopsis thaliana*. RNA Biol. **13**:441–454.

Pendle, A.F., Clark, G.P., Boon, R., Lewandowska, D., Lam, Y.W., Andersen, J., Mann, M., Lamond, A.I., Brown, J.W., and Shaw, P.J. (2005). Proteomic analysis of the *Arabidopsis* nucleolus suggests novel nucleolar functions. Mol. Biol. Cell **16**:260–269.

Perreault, A., Bellemer, C., and Bachand, F. (2008). Nuclear export competence of pre-40S subunits in fission yeast requires the ribosomal protein Rps2. Nucleic Acids Res. **36**:6132–6142.

Perreault, A., Gascon, S., D'Amours, A., Aletta, J.M., and Bachand, F. (2009). A methyltransferase-independent function for Rmt3 in ribosomal subunit homeostasis. J. Biol. Chem. **284**:15026–15037.

Pontvianne, F., Matia, I., Douet, J., Tourmente, S., Medina, F.J., Echeverria, M., and Saez-Vásquez, J. (2007). Characterization of AtNUC-L1 reveals a central role of nucleolin in nucleolus organization and silencing of AtNUC-L2 gene in *Arabidopsis*. Mol. Biol. Cell **18**:369–379.

Pillet, B., Mitterer, V., Kressler, D., and Pertschy, B. (2017). Hold on to your friends: dedicated chaperones of ribosomal proteins. BioEssays **39**:1–12.

Robinson, M.D., McCarthy, D.J., and Smyth, G.K. (2010). edgeR: a Bioconductor package for differential expression analysis of digital gene expression data. Bioinformatics **26**:139–140.

Rosado, A., Sohn, E.J., Drakakaki, G., Pan, S.Q., Swidergal, A., Xiong, Y.Q., Kang, B.H., Bressan, R.A., and Raikhel, N.V. (2010). Auxin-mediated ribosomal biogenesis regulates vacuolar trafficking in *Arabidopsis*. Plant Cell **22**:143–158.

Sáez-Vásquez, J., Caparros-Ruiz, D., Barneche, F., and Echeverria, M. (2004a). Characterization of a crucifer plant pre-rRNA processing complex. Biochem. Soc. Trans. **32**:578–580.

Sáez-Vásquez, J., Caparros-Ruiz, D., Barneche, F., and Echeverria, M. (2004b). A plant snoRNP complex containing snoRNAs, fibrillarin, and nucleolin-like proteins is competent for both rRNA gene binding and pre-rRNA processing in vitro. Mol. Cell Biol. **24**:7284–7297.

Sáez-Vásquez, J., and Delseny, M. (2019). Ribosome biogenesis in plants: from functional 45S ribosomal DNA organization to ribosome assembly factors. Plant Cell **31**:1945–1967.

Samaha, H., Delorme, V., Pontvianne, F., Cooke, R., Delalande, F., Van Dorsselaer, A., Echeverria, M., and Sáez-Vásquez, J. (2010). Identification of protein factors and U3 snoRNAs from a Brassica oleracea RNP complex involved in the processing of pre-rRNA. Plant J. **61**:383–398.

Sawyer, I.A., Sturgill, D., and Dundr, M. (2019). Membraneless nuclear organelles and the search for phases within phases. Wiley Interdiscip. Rev. RNA **10**:e1514.

Sharma, K., and Tollervey, D. (1999). Base pairing between U3 small nucleolar RNA and the 5′ end of 18S rRNA is required for pre-rRNA processing. Mol. Cell Biol. **19**:6012–6019.

Shaw, P., and Brown, J. (2012). Nucleoli: composition, function, and dynamics. Plant Physiol. **158**:44–51.

Shi, D., Liu, J., Xiang, Y., Ye, D., Sundaresan, V., and Yang, W. (2005). SLOW WALKER1, essential for gametogenesis in *Arabidopsis*, encodes a WD40 protein involved in 18S ribosomal RNA biogenesis. Plant Cell **17**:2340–2354.

Swiercz, R., Cheng, D., Kim, D., and Bedford, M.T. (2007). Ribosomal protein rpS2 is hypomethylated in PRMT3-deficient mice. J. Biol. Chem. **282**:16917–16923.

Swiercz, R., Person, M.D., and Bedford, M.T. (2005). Ribosomal protein S2 is a substrate for mammalian PRMT3 (protein arginine methyltransferase 3). Biochem. J. **386**:85–91.

Tamura, K., Stecher, G., Peterson, D., Filipski, A., and Kumar, S. (2013). MEGA6: molecular evolutionary genetics analysis version 6.0. Mol. Biol. Evol. **30**:2725–2729.

Tang, J., Gary, J.D., Clarke, S., and Herschman, H.R. (1998). PRMT3, a type I protein arginine N-methyltransferase that differs from PRMT1 in its oligomerization, subcellular localization, substrate specificity, and regulation. J. Biol. Chem. **273**:16935–16945.

Thomson, E., Ferreira-Cerca, S., and Hurt, E. (2013). Eukaryotic ribosome biogenesis at a glance. J. Cell Sci. **126**:4815–4821.

Tomecki, R., Sikorski, P.J., and Zakrzewska-Placzek, M. (2017). Comparison of preribosomal RNA processing pathways in yeast, plant and human cells - focus on coordinated action of endo- and exoribonucleases. FEBS Lett. **591**:1801–1850.

Tsutsui, H., and Higashiyama, T. (2017). pKAMA-ITACHI vectors for highly efficient CRISPR/Cas9-Mediated gene knockout in *Arabidopsis thaliana*. Plant Cell Physiol. **58**:46–56.

Wang, D., Qin, B., Li, X., Tang, D., Zhang, Y., Cheng, Z., and Xue, Y. (2016). Nucleolar DEAD-box RNA helicase TOGR1 regulates thermotolerant growth as a pre-rRNA chaperone in rice. PLoS Genet. **12**:e1005844.

Wang, Z., Xing, H., Dong, L., Zhang, H., Han, C., Wang, X., and Chen, Q. (2015). Egg cell-specific promoter-controlled CRISPR/Cas9 efficiently generates homozygous mutants for multiple target genes in *Arabidopsis* in a single generation. Genome Biol. **16**:144.

Watkins, N.J., and Bohnsack, M.T. (2012). The box C/D and H/ACA snoRNPs: key players in the modification, processing and the dynamic folding of ribosomal RNA. Wiley Interdiscip. Rev. RNA **3**:397–414.

Weis, B.L., Kovacevic, J., Missbach, S., and Schleiff, E. (2015a). Plant-specific features of ribosome biogenesis. Trends Plant Sci. **20**:729–740.

Weis, B.L., Palm, D., Missbach, S., Bohnsack, M.T., and Schleiff, E. (2015b). atBRX1-1 and atBRX1-2 are involved in an alternative rRNA processing pathway in *Arabidopsis thaliana*. RNA **21**:415–425.

Woolford, J.L., Jr., and Baserga, S.J. (2013). Ribosome biogenesis in the yeast *Saccharomyces cerevisiae*. Genetics **195**:643–681.

Yao, R., Xu, G., Wang, Y., Shan, L., Luan, P., Wang, Y., Wu, M., Yang, L., Xing, Y., Yang, L., et al. (2019). Nascent pre-rRNA sorting via phase separation drives the assembly of dense fibrillar components in the human nucleolus. Mol. Cell **76**:767–783.

Zhang, L., Wu, C., Cai, G., Chen, S., and Ye, K. (2016). Stepwise and dynamic assembly of the earliest precursors of small ribosomal subunits in yeast. Genes Dev. **30**:718–732.

Zhang, B., Wang, L., Zeng, L., Zhang, C., and Ma, H. (2015). *Arabidopsis* TOE proteins convey a photoperiodic signal to antagonize CONSTANS and regulate flowering time. Genes Dev. **29**:975–987.

Zhang, B., You, C., Zhang, Y., Zeng, L., Hu, J., Zhao, M., and Chen, X. (2020). Linking key steps of microRNA biogenesis by TREX-2 and the nuclear pore complex in *Arabidopsis*. Nat. Plants **6**:957–969.

Zhang, Y., and Lu, H. (2009). Signaling to p53: ribosomal proteins find their way. Cancer Cell **16**:369–377.

Zhao, T., Huan, Q., Sun, J., Liu, C., Hou, X., Yu, X., Silverman, I.M., Zhang, Y., Gregory, B.D., Liu, C., et al. (2019). Impact of poly(A)-tail G-content on *Arabidopsis* PAB binding and their role in enhancing translational efficiency. Genome Biol. **20**:189.

Zhou, Y., Zhou, B., Pache, L., Chang, M., Khodabakhshi, A.H., Tanaseichuk, O., Benner, C., and Chanda, S.K. (2019). Metascape provides a biologist-oriented resource for the analysis of systems-level datasets. Nat. Commun. **10**:1523.

Zhu, P., Wang, Y.Q., Qin, N., Wang, F., Wang, J., Deng, X., and Zhu, D. (2016). *Arabidopsis* small nucleolar RNA monitors the efficient pre-rRNA processing during ribosome biogenesis. Proc. Natl. Acad. Sci. U S A **113**:11967–11972.